Evaluation of the self-healing effect in cement-based materials with embedded cementitious capsules by means of Acoustic Emission techniques

Evaluation of the self-healing effect in cement-based materials with embedded cementitious capsules by means of Acoustic Emission techniques

Giovanni Anglani[1], *Pedro* Marin Montanari[1]. *Jean Marc* Tulliani[2], *Giuseppe* Lacidogna[1*], and *Paola* Antonaci[1]

[1]Department of Structural, Geotechnical and Building Engineering, Politecnico di Torino, Corso Duca degli Abruzzi 24, 10129 Torino, Italy
[2] Department of Applied Science and Technology, INSTM R.U PoliTO-LINCE Laboratory, Politecnico di Torino, Corso Duca degli Abruzzi 24, 10129 Torino, Italy

Abstract. Due to its low tensile strength and the presence of defects brought on by improper construction methods or other factors, cracks in concrete are practically inevitable. For reinforced-concrete structures, even if cracks do not necessarily increase the risk of collapse, they unquestionably hinder aspects such as service life. Self-healing cementitious materials have been developed because of growing concern for the security and sustainability of structures. For these new materials to be used in actual structures, it is essential to conduct research into the self-repair effect that they may offer, and possibly quantify it directly on-site, by means of non-destructive methods. In this sense, the objective of this work is to use Acoustic Emission (AE) analyses to non-destructively characterise the response of an autonomic capsule-based system, as a function of the specific polymeric healing agents contained in the capsules. Comparisons will be made between the reference and self-healing specimens, and between the different self-healing specimens themselves, through the analysis of such parameters as the ultimate load, absorbed fracture energy, and emitted Acoustic Emission (AE) energy. Such type of analysis can give valuable insights not only on quantitative but also on qualitative aspects (such as the level of brittleness or ductility introduced by the specific self-healing system adopted) in view of possible applications in real structures.

1 Introduction

The appearance of cracks in concrete is almost unavoidable due to its low tensile strength and the presence of defects resulting from an incorrect execution, shrinkage, or other causes. While the presence of cracks does not necessarily pose a risk of collapse for concrete structures, they surely impair their functionality, accelerating their degradation and diminishing their service life. The increasing concern for the safety and sustainability of concrete structures led to the study and development of smart self-healing cementitious materials [1,2]. The assurance of the repair offered by the self-healing effect is a crucial issue to safely implement these novel materials in real structures. For this reason, several characterization methodologies were proposed in the past decades to evaluate the effectiveness of the different proposed self-healing technologies with reference to one or more material properties [3]. When studying the self-healing properties of construction materials, an important contribution can be achieved through the use of different nondestructive testing (NDT) techniques [3,4]. For this purpose, several NDT techniques were successfully used, such as ultrasonic [5–12] or AE techniques [12–20].

The aim of this study is to use AE techniques to investigate the behavior of an autonomic self-healing system based on the use of cementitious macro-capsules embedded in a cementitious matrix. The cementitious capsules were proved effective in protecting and correctly releasing several healing agents from the main types commonly used (i.e., minerals, polymerics, and bacterial agents) [21], offering a good recovery in terms of durability-related properties and also mechanical resistance, both in case of static and fatigue loadings [22]. Moreover, the cementitious capsules present inherent compatibility with the surrounding matrix and the potential to sustain the mixing process. Given these promising aspects, the AE techniques will be used to further investigate the proposed autonomic system behavior, with the aim to define features that could be useful to assess the activation of the self-healing effect and to evaluate the self-healing system properties during damage and the successive recovery, in view of its future scale-up to real-scale structures.

* Corresponding author: giuseppe.lacidogna@polito.it

2 Materials and Methods

Regarding the healing agents, two different types were used – both were single-component polyurethane (PU) resins produced from Minova CarboTech GmbH (Germany), Carbostop U and Carbostop F [23,24]. Both resins cure when in contact with moisture from air or from mortars, but differ in their viscosity, foaming factor, and presence/absence of an integral catalyst [23,24]. To prevent any undesired polymerization before the tests, the resins were encapsulated in well-sealed cementitious capsules with an internal diameter of 5.5 mm, an outer diameter of 8 mm, and a length of 55 mm. Samples containing the capsules with the resin Carbostop U were labelled as PUC, while the ones with the resin Carbostop F were labelled as PUF. The PUC resin was accelerated and highly expansive, whereas the PUF resin was not accelerated and was slightly expansive. Finally, the reference samples without any capsule were referred as REF. The cementitious capsules were manufactured using a polymer-modified cement paste according to previous experiences [22].

The mixing was done in accordance with [22]. After mixing with an overhead stirrer (RW 20, IKA, Germany), the fresh cement paste was rolled around an oiled bar, leading to a smooth cementitious tube with a hollow circular cross-section. The bar was then removed, and the cementitious tubes were kept for 7 days in a humid environment (T ~ 20 C and relative humidity (RH) ~95%) prior to being exposed to air (T ~ 20 C, 50-60% RH) for complete curing over 28 days. Then, the tubes were cut to the desired length. Subsequently, an epoxy coating (Plastigel, API SpA, Italy) was applied to the internal surface of the tubes. This epoxy coating was mandatory to guarantee water tightness to the capsule, and to avoid any premature curing of the resins with moisture present in the fresh mortar mixes. One end of the tubular capsule was sealed with a two-component epoxy plaster (Stucco K, API SpA, Italy) before filling it with the PU resin. Finally, the second end was immediately sealed with the epoxy plaster after filling, to limit the contact time of the healing agent with surrounding atmosphere.

Regarding the specimens, they had dimensions (40 × 40 × 160 mm^3) and were produced with a standardized mortar mix composition, in agreement with EN 196-1. Portland cement (CEM II 42.5 A/LL, Buzzi Unicem S.p.A., Italy), normalized sand (grading 0–2 mm, DIN EN 196-1), and tap water were used. The water to cement ratio was equal to 0.50, while the sand to cement ratio was 3. In the PUC and PUF series, one capsule containing the healing agent was fixed in the center of the mold by means of a nylon thread, at about one third in height. A notch was also created in the samples, by means of a removable plastic element inserted at the bottom of the molds. The notch width and notch height were equal to 4 mm.

The specimens also had a longitudinal hole of diameter 5 mm, with the center positioned at 15 mm from the upper face, 25 mm from the lower face. The creation of a longitudinal hole is related to the setup for additional permeability analyses, that have been performed on the same specimens by means of water-flow tests [25]. The results of these tests are not included in this paper for the sake of brevity, considering the focus on Acoustic Emission. However, the detail regarding the longitudinal hole is included in the specimen description because it may have an influence on the cracking process and in the related AE analyses.

The molds were filled in two layers and each layer was compacted on a jolting table by 60 jolts. In addition, the molds were covered with plastic foils until demolding, the day after casting. Finally, the samples were cured in a humidity-saturated environment for 1 week. Figure 1 shows the cross-section of a broken PUC specimen highlighting the capsule cross-section and the polyurethane foam partially covering the crack surface.

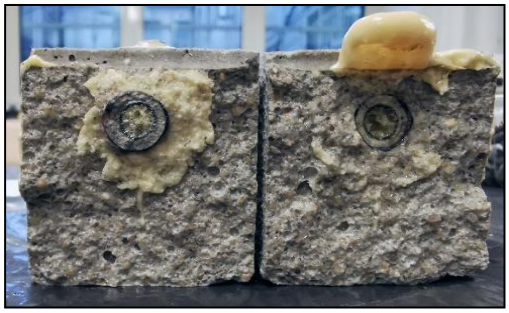

Fig. 1. Cross-section of a PUC specimen after failure showcasing the ruptured resin capsule and the the spilled resin.

Regarding the testing procedure, static three-point bending tests were carried out in two phases. They were conducted using a servo-controlled machine (MTS) with a maximum capacity of 250 kN and load measurement accuracy of ± 1.0%. This machine is equipped with control electronics which makes it possible conduct tests in either load control or displacement control. All the tests were also carried out with the simultaneous acquisition of Acoustic Emission (AE) signals.

The first phase was pre-cracking tests, i.e., static tests on virgin REF, PUC, and PUF specimens, performed by Crack Mouth Opening Displacement Control (CMOD) up to a target displacement of approx. 800 microns under load. The device used for the CMOD control was a DD1 clip-on gauge manufactured by the HBM, placed on the lower face of the specimen across the notch. For all tests, the specimens mid-span deflection was also measured using the MTS piston vertical stroke.

The second testing phase was the static reloading tests for the self-repaired specimens – performed under the same conditions as the first phase. Only PUCs and PUFs were subjected to the second phase because the REFs had no load-bearing capabilities after the pre-cracking tests.

It was not possible to obtain a repeatable residual crack width value for every specimen due to their different mechanical response to the pre-cracking procedure.

In total, 6 REF, 8 PUC and 14 PUF (in their virgin state), 6 PUC, and 2 PUF (in their self-repaired state) were analyzed via AE, for a total of 36 samples. Figure 2 shows the placement of the specimen in the MTS testing machine frame and the position of the AE sensors.

Regarding the AE data acquisition, two Lunitek "AEmission" sensors were used (model LT18-003-PRD-00-R0) with a frequency range of 15-625 kHz. They were mounted on the top face of the testing specimen, vertically aligned with the supports. The sensors were attached to each specimen using plasticine. The data acquisition system used a 5 MHz sampling frequency and stored data in parametric form [14].

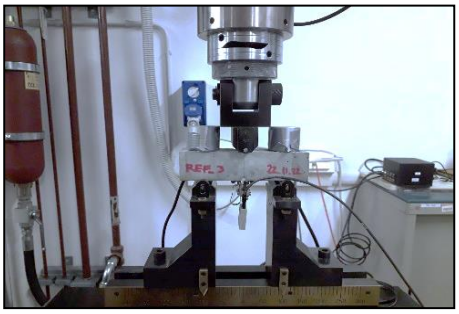

Fig. 2. Testing procedure on the MTS testing machine of a reference (REF) sample showing the placement of the AE sensors.

The recorded parameters for each detected signal were:

- Signal start time: instant of the first reading that exceeds the detection threshold: 49 dB (280 μV)
- Peak amplitude, expressed in dB (AdB = 20log10 (Vmax/1 μV));
- Number of oscillations (counts): the number of intermediate crossings of the threshold by the signal. This measure is also commonly used to estimate the AE signal's average frequency (AF) through the counts/duration relationship (signal duration ≡ end time–start time);
- AE energy (E_{AE}): integral of the waveform, as indicated by RILEM [26]. When the acquisition of the signal is parametric, it can be approximated by the half of the rectangle formed by the signal peak amplitude and its duration [27–29].

The AE signals energy was calculated according to Eq.1.

$$E_{AE} = \sum_{i=1}^{N} \frac{A_i \times \Delta t_i}{2} \text{ [mVs]} \quad (1)$$

where "A_i" is the signal amplitude [mV] of the signal i, "N" is the number of AE signals, and "Δt" is the signal duration [s]. The "W_0" energy was calculated, according to the RILEM TC-50 FMC [30], as the area under the load-displacement curve, obtained via the trapezium rule, according to Eq. 2.

$$W_0 = \sum_{i=2}^{M} (\delta_i - \delta_{i-1}) \left(\frac{F_i + F_{i-1}}{2}\right) \text{ [J]} \quad (2)$$

where " δ " is the relative displacement [m] measured by the CMOD sensor placed at mid-span of the specimen, "M" is the number of measured data points, and "F" is the load [N]. Examples of the load-displacement curve of virgin and self-repaired specimens will be shown in the following section.

The fracture energy was then calculated by dividing the "W_0" energy by the ligament area, according to Eq. 3 [30].

$$G_f = \frac{W_0}{S_L} \text{ [N/m]} \quad (3)$$

where "W_0" is the total energy of Eq. 2, calculated in J, and "S_L" is the specimen ligament area in m^2 (the specimens had dimensions (40 × 40 × 160) mm^3 and the notch width and height were equal to 4 mm, making the ligament area equal to (40 × 36) mm^2, see section 2).

3 Results and Discussion

The rate and cumulated AE signals for a virgin and a self-repaired PUC specimen are shown in Figures 3 and 4.

As expected, the peak load sustained by the virgin PUC specimen is higher with respect to the self-repaired one. Most AE signals occur in the beginning of the test with the generation of micro-cracks. An example of the load-displacement curve used to calculate the fracture energy is shown in Figure 5 (for a PUC specimen in the virgin state) The same procedure was performed for the self-repaired specimen, as well as for all the other specimens.

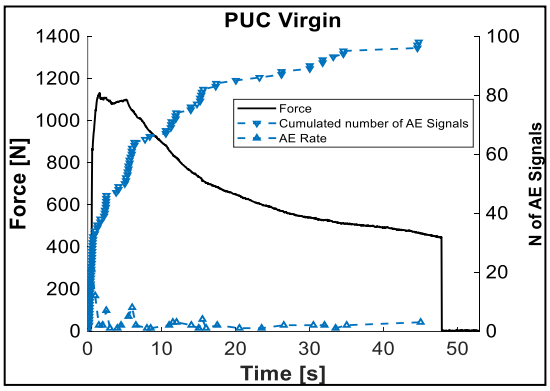

Fig. 3. Rate and cumulated AE signals on a virgin PUC specimen

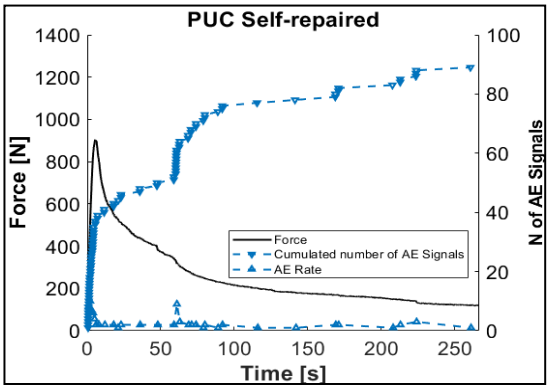

Fig. 4. Rate and cumulated AE signals on a self-repaired PUC specimen

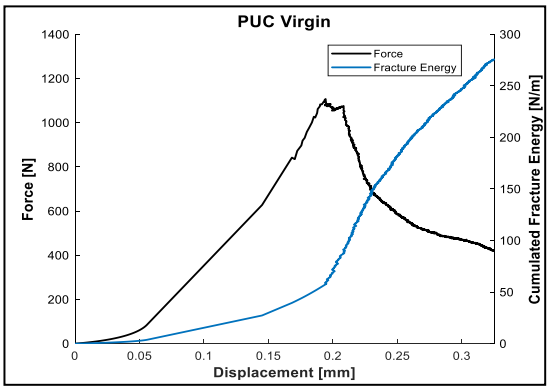

Fig. 5 Load-Displacement curve of a PUC specimen in the virgin state

The rate and cumulated AE signals for a virgin and a self-repaired PUF specimen are shown in Figures 6 and 7. Also in this case, the peak load sustained by the original specimen is higher with respect to the self-repaired one. The load-displacement curve used to calculate the fracture energy is shown in Figure 8.

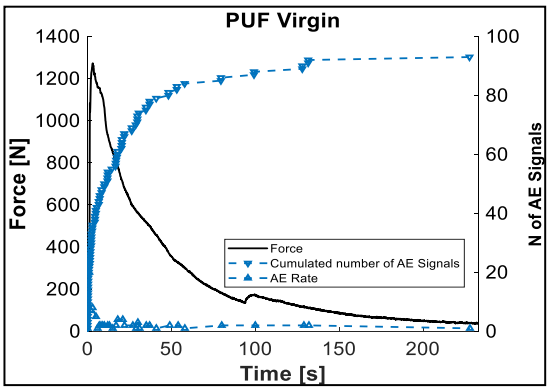

Fig. 6. Rate and cumulated AE signals on a virgin PUF specimen

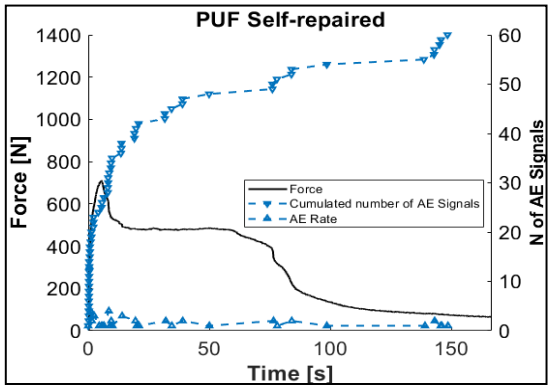

Fig. 7. Rate and cumulated AE signals on a self-repaired PUF specimen

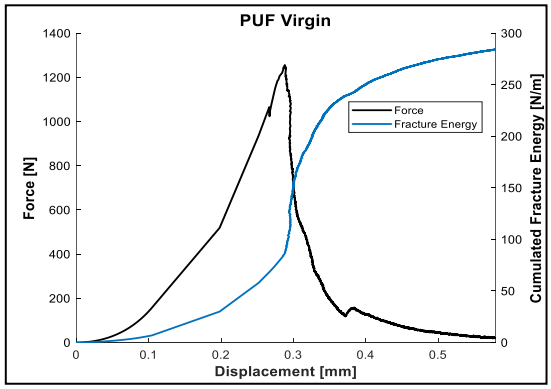

Fig. 8. Load-displacement curve of a virgin PUF specimen

A synthesis of the peak load and fracture energy values obtained from the tests can be seen in Figures 9 and 10. Figure 9 shows that the higher peak load values are associated with the virgin REF specimens. The dashed lines indicate the average. Figure 10 demonstrates that the higher fracture energy values are associated with the virgin specimens PUC and PUF.

Figures 11 and 12 show the relation between peak load and fracture energy for the virgin and self-repaired specimens, respectively. The dashed lines indicate the trend.

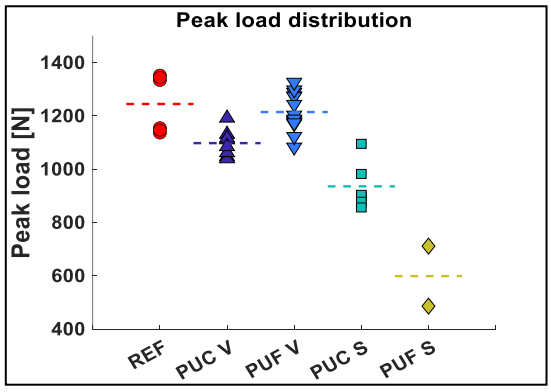

Fig. 9 Peak load distribution of all the specimens

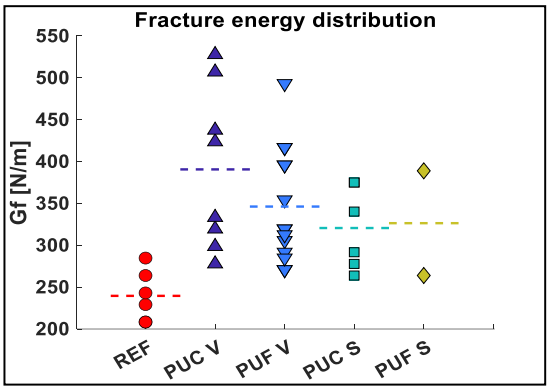

Fig. 10. Fracture energy distribution of all the specimens

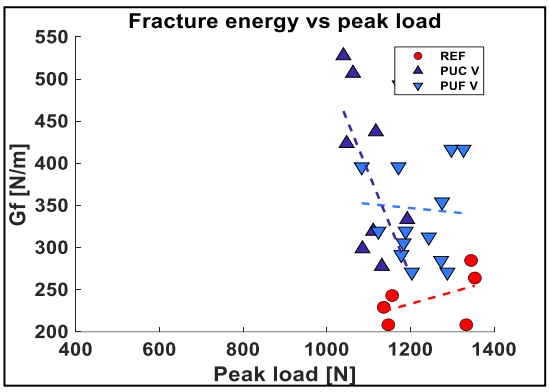

Fig. 11. Fracture energy vs peak load of the virgin REF, PUC and PUF specimens

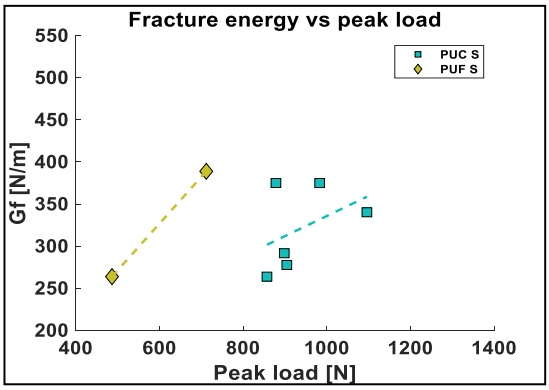

Fig. 12. Fracture energy vs peak load of the self-repaired PUC and PUF specimens

From Figure 11 it can be observed that the virgin PUC and PUF specimens behave in a brittle way – because as the force increases, the absorbed fracture energy decreases. The REF specimens behave differently, in a ductile way, showing an increasing relationship between fracture energy and peak load. This difference is possibly caused by disturbances created in the PUC and PUF specimens' body by the capsules. Furthermore, from Figure 12, it can be seen that the self-repaired PUC and PUF specimens also have a ductile behavior, as their fracture energy absorption ability increases with the load-bearing capacity.

A loading process envisions the distribution of the released energy as the sum of the absorbed or dissipated (fracture) energy and the emitted (AE) energy, as evidenced in [28]. Therefore, considering that toughness is the amount of energy that a material can absorb before collapsing, it can be inferred that the self-repaired PUC specimens are tougher than the original ones since, considering the same fracture energy (absorbed energy), they tend to have lower AE energy values (emitted energy), as can be seen from Figure 13. This is probably due to the fact that the self-repaired PUC specimens center section has a more elastic behavior than the rest of the body.

This analysis was made only with PUC specimens because of lack of sufficient data for statistical analysis of PUF specimens regarding the AE energy.

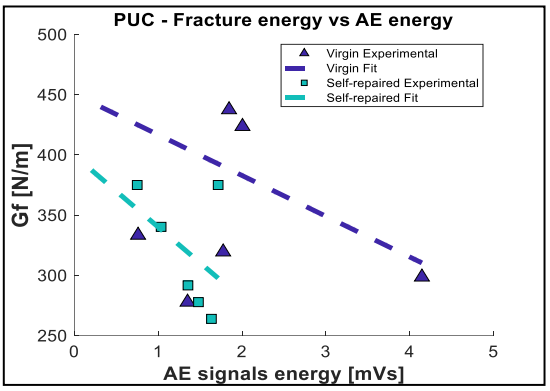

Fig. 13. Fracture energy vs AE energy of the PUC specimens

4 Conclusions

In this work, cementitious-shell and polyurethane-core macro-capsules embedded in standardized mortar mix specimens have been used as an example of an autonomic capsule-based self-healing system for cementitious materials.

Static CMOD-controlled three-point bending tests were performed to pre-crack the samples and trigger the self-healing mechanism. Identical tests were conducted after self-repair to quantify the mechanical regain. Acoustic emission (AE) signals were acquired during the tests. In total 36 specimens where tested, which is a sufficient number to carry out preliminary but not definitive analyses.

The peak load and the fracture energy distribution were calculated for all the tests (Figures 9 and 10). Furthermore, the correlations between the fracture energy and the peak loads were considered for all the specimens (Figures 11 and 12). For some specimens the correlations between fracture energy and AE energy were also highlighted (Figure 13).

The tests emphasize that the self-healing effect due to the polymeric healing agents used generate a transition from brittle to ductile behavior. As a matter of fact, on the original samples there is an inverse correlation between fracture energy and peak load (Figure 11), whereas in the self-repaired specimens the correlation is direct (Figure 12), showing an increasing relation between fracture energy and peak load. Finally, for the PUC specimens it can be verified that self-repaired samples are tougher than the original ones, since, considering the same fracture energy (absorbed energy), they present lower AE energy values (emitted energy) (Figure 13).

Additional tests will be conducted to confirm these preliminary results, further enhancing the statistical analyses.

References

[1] N. De Belie, E. Gruyaert, A. Al-Tabbaa, P. Antonaci, C. Baera, D. Bajare, et al. Adv Mater Interfaces. **5**, 1800074 (2018).
[2] K. Van Tittelboom, N. De Belie. Materials. **6**, 2182–2217 (2013).
[3] L. Ferrara, T. Van Mullem, M.C. Alonso, P. Antonaci, R.P. Borg, E. Cuenca, et al. Constr Build Mater. **167**, 115– 142 (2018)
[4] D. Snoeck, F. Malm, V. Cnudde, C.U. Grosse, K. Van Tittelboom. Adv Mater Interfaces. **5**, 1800179 (2018).
[5] C.M. Aldea, W.J. Song, J.S Popovics, S.P Shah. J. Mater Civ Eng. **12**, 92-96 (2000).
[6] K. Van Tittelboom, N. De Belie, W. De Muynck, W. Verstraete. Cem Concr Res. **40**, 157–166 (2010).
[7] L. Ferrara, V. Krelani, M. Carsana. Constr Build Mater. **68**, 535–551 (2014).
[8] R. Alghamri, A. Kanellopoulos, A. Al-Tabbaa. Constr Build Mater. **124**, 910–921 (2016).
[9] Hilloulin B, Legland J-B, Lys E, Abraham O, Loukili A, Grondin F, et al. Constr Build Mater. **123**, 143–152 (2016).
[10] M. Ait Ouarabi, P. Antonaci, F. Boubenider, A. Gliozzi, M. Scalerandi. Materials. **10**, 46 (2017)
[11] AS. Gliozzi, M. Scalerandi, G. Anglani, P. Antonaci, L. Salini. Phys Rev Mater. **2**, 13601 (2018)
[12] G. Lefever, D. Snoeck, N. De Belie, S. Van Vlierberghe, D. Van Hemelrijck, DG. Aggelis. Sensors. **20**, 2959 (2020).
[13] K. Van Tittelboom, J. Wang, M. Araújo, D. Snoeck, E. Gruyaert, B. Debbaut, et al. Constr Build Mater. **107**, 125–137 (2016).
[14] P. Minnebo, G. Thierens, G. De Valck, K. Van Tittelboom, N. De Belie, D. Van Hemelrijck, et al. Materials. **10**, 49 (2017).
[15] E. Tsangouri, G. Karaiskos, A. Deraemaeker, D. Van Hemelrijck, D. Aggelis. Constr Build Mater. **129**, 163–171 (2016).
[16] J. Feiteira, E. Tsangouri, E. Gruyaert, C. Lors, G. Louis, N. De Belie. Mater Des. **115**, 238–46 (2017).
[17] K. Van Tittelboom, E. Tsangouri, D. Van Hemelrijck, N. De Belie. Cem Concr Compos. **57**, 142–152 (2015).
[18] E. Tsangouri, FA. Gilabert, N. De Belie, D. Van Hemelrijck, X. Zhu, DG Aggelis. Constr Build Mater. **218**, 424–433 (2019).
[19] E. Tsangouri, J. Lelon, P. Minnebo, H. Asaue, T. Shiotani, K. Van Tittelboom, et al. Constr Build Mater. **228**, 116780 (2019).
[20] E. Tsangouri, DG Aggelis, K. Van Tittelboom, N. De Belie, D. Van Hemelrijck. Sci World J. **2013**, 1–10 (2013).
[21] G. Anglani, T. Van Mullem, X. Zhu, J. Wang, P. Antonaci, N. De Belie, et al. Constr Build Mater. **251**, 119039 (2020).
[22] G. Anglani, J-M. Tulliani, P. Antonaci. Materials. **13**, 1149 **(**2020).
[23] TECHNICAL DATA SHEET - CARBOSTOP U n.d. https://www.minovaglobal.com/media/1663/carbostop-u-tds.pdf (accessed January 25, 2023).
[24] TECHNICAL DATA SHEET - CARBOSTOP F n.d. https://www.minovaglobal.com/media/1673/carbostop-f-tds.pdf (accessed January 25, 2023).
[25] T. Van Mullem, G. Anglani, M. Dudek, H. Vanoutrive, G. Bumanis, C. Litina, et al. Sci Technol Adv Mater. **21**, 661–682 (2020).
[26] RILEM Technical Committee (Masayasu Ohtsu). Mater Struct. 43, 1187–9 (2010).
[27] LF. Friedrich, BNR. Tanzi, AB. Colpo, M. Sobczyk, G. Lacidogna, G. Niccolini, et al. Appl Sci Switz. **12**, 1980 (2022).
[28] A. Carpinteri, G. Lacidogna, M. Corrado, E. Di Battista. Eng Fract Mech. **155**, 130–144 (2016).
[29] X. Liu, Q. Liu, B. Liu, Q. Liu. J Geophys Eng. **16**, 1164–1177 (2019)
[30] Recommendation (50-FMC) RD. Mater Struct. **18**, 285–190 (1985).